Science
AAAS

Supplementary Materials for

Imaging Dynamic and Selective Low-Complexity Domain Interactions That Control Gene Transcription

Shasha Chong, Claire Dugast-Darzacq, Zhe Liu, Peng Dong, Gina M. Dailey, Claudia Cattoglio, Alec Heckert, Sambashiva Banala, Luke Lavis, Xavier Darzacq, Robert Tjian*

correspondence to: jmlim@berkeley.edu

This PDF file includes:

Other Supplementary Materials for this manuscript include the following:

Materials and Methods:

Cell culture, stable cell line construction and imaging sample preparation

Human U2OS cells containing a LacO array (#1, 2 or 3) in the genome were grown in low-glucose DMEM (ThermoFisher, 10567014) with 10% fetal bovine serum (HyClone FBS SH30910.03) and 1% penicillin-streptomycin (ThermoFisher, 15140122). Cell line 1 containing ~50,000 LacO elements in the array was described in Janicki *et al*. *(25)*. Cell line 2 containing ~15,000 LacO elements in the array was created by co-transfecting 3 plasmids: the first encoding puromycin selection cassette, the second containing 256 LacO repeats and the third containing the luciferase-CFP-24×MS2 fusion reporter gene under the control of 7 TetO elements and a CMV promoter. Cell line 3 contains ~40,000 LacO elements in the array that were inserted in tandem in quasi-absence of any other regulation element (*e.g.* promoter). This line was described in *(46)*. The number of integrated LacO repeats was quantified by qPCR using 2 different pairs of oligonucleotides priming (either before or after the tandem LacO) once per integrated LacO repeats-containing plasmid (Table S4). We also used the plasmid pBslacO for an absolute quantification of the number of plasmids integrated per genome (for our calculation we estimated the amount of DNA per cell to be 6 pg). The calculation details are included in Table S5.

Human A673 Ewing's sarcoma cells (ATCC® CRL-1598) and 293T cells (ATCC® CRL-3216) were grown in high-glucose DMEM (ThermoFisher, 10566016) with 10% FBS and 1% penicillin-streptomycin. For live-cell imaging, the medium was identical except that phenol-red-free DMEM (ThermoFisher, 31053028) was used. U2OS, A673 and 293T cells were cultured at 37°C with 5% CO_2.

The A673 cell line stably expressing H2B-Halo was generated using PiggyBac transposition and drug selection. This cell line was used in the SPT experiments to correct for dye photobleaching and axial cell or chromatin drift. Briefly, the cDNA encoding H2B-Halo was cloned into a PiggyBac vector co-expressing a G418 resistance gene, and this vector was co-transfected together with a SuperPiggyBac transposase vector into the A673 cell line using Fugene 6 (Promega, E2691) according to the manufacturer's instructions. 48 hours after transfection, we started with selection by adding 0.5 mg/ml G418. Untransfected A673 cells were treated with G418 in parallel, and selection was judged to be complete once no untransfected cells remained (~ 1 week). The cells were further selected for 2 weeks under 0.25 mg/ml G418 before stocks were frozen.

The construction of U2OS cell line stably expressing H2B-Halo was described in *(24)*. The LacO-array-containing U2OS cell line 2 stably expressing Halo-RPB1 was generated using an α-amanitin resistant expression vector encoding an N-terminally Halo-tagged α-amanitin resistant (N792D) RPB1. Briefly, cells were transfected using Fugene 6 following manufacturer's instruction, α-amanitin (Sigma, A2263) was used during the stable selection process at a concentration of 2 μg/ml and was used thereafter in permanence in the culture of the cells at a concentration of 1 μg/ml to avoid endogenous RPB1 re-expression as described in *(47)*.

The EWS/FLI1 knockout A673 cell lines stably expressing exogenous EWS/FLI1 or EWS(YS)/FLI1 were generated using PiggyBac transposition and drug selection following the

same protocol used for generating the A673 line stably expressing H2B-Halo. The PiggyBac vector co-expresses a puromycin resistance gene. The transfected cells were selected with puromycin (1 μg/μl) for over 2 weeks before stocks were frozen.

For live-cell single-molecule imaging, the cells were plated on 25 mm circular No. 1 cover glasses (Azer Scientific, 200251) that were plasma-cleaned prior to use. To image transiently expressed proteins, we transfected the cells with the target construct using Fugene 6, then grew them for 24 hours. To image stably expressed proteins, we grew the cells on the cover glasses overnight for sample preparation. The cells were then labeled with relevant HaloTag or $SNAP_f$-tag dyes at the indicated concentration for 15 min (Halo) or 30 min ($SNAP_f$) and washed twice (for each wash: remove medium, rinse twice with PBS, incubate in fresh medium for 30 min). At the end of the final wash, the medium was changed to phenol-red-free imaging medium as described above.

The same protocol was followed to prepare fixed cell samples for confocal fluorescence imaging, except that the cells were grown on 18 mm circular No. 1 cover glasses (VWR VistaVision, 16004-300). For FRAP experiment and live-cell imaging during hexanediol treatment, sample preparation was identical except that cells were grown on glass-bottom (No. 1.5, 14 mm diameter) 35 mm dishes (MatTek, P35G-1.5-14-C) and not labeled with dyes when EYFP or mCherry fluorescence was monitored.

CRISPR/Cas9-mediated genome editing

We created knock-in and knockout cell lines roughly according to published procedures *(36)*, except exploiting the HaloTag in fluorescence-activated cell sorting (FACS) for EWS/FLI1-Halo knock-in cells.

To create EWS/FLI1 knockout cells, we transfected A673 cells with a Cas9 plasmid. The Cas9 plasmid was slightly modified from that distributed from the Zhang lab *(36)*: 3xFLAG-SV40NLS-pSpCas9 was expressed from a CBh promoter; the sgRNA was expressed from a U6 promoter; and mVenus was expressed from a PGK promoter. To create EWS/FLI1-Halo knock-in cells, we co-transfected A673 using a repair plasmid together with the Cas9 plasmid (3:1 mass ratio for repair plasmid to Cas9 plasmid). For the repair vector, we modified a pUC57 plasmid to incorporate coding sequences for TEV protease recognition epitope (EDLYFQS), HaloTag and FLAG-tag flanked by ~750 bp of genomic homology sequence (homology arm) of FLI1 C-terminus on either side. The TEV linker sequence was between FLI1 and HaloTag. Since the wild-type A673 does not express the wild-type FLI1 *(33)*, only the endogenous EWS/FLI1 was tagged and expressed in the knock-in A673. We introduced synonymous mutations (last 11 codons of FLI1 before TAG) in the homology sequence, where necessary, to prevent the Cas9-sgRNA complex from cutting the repair vector.

In each case, we designed two or three sgRNAs using the Zhang lab CRISPR design tool (http://tools.genome-engineering.org), cloned them into the Cas9 plasmid and transfected A673 using individual Cas9-sgRNA plasmid only (for knockout) or together with the repair vector (for knock-in). 24 hours after transfection, we then pooled cells transfected with each of the sgRNAs individually and FACS-sorted for YFP (mVenus) positive, successfully transfected cells. To generate the HaloTag knock-in, we grew the YFP-positive cells for 19 days, labeled them with

500 nM HaloTag TMR ligand (Promega, G8251), FACS-sorted for HaloTag-positive cells and plated one cell per well into 96-well plates. To generate EWS/FLI1 knockout, we similarly grew up the YFP-positive cells and plated single cells in 96-well plates via FACS.

Clones were then expanded and screened by genomic PCR (for knock-in, using a genomic primer external to the homology sequence and an internal HaloTag primer) or western blot (for knockout). Successfully edited clones were further verified with western blot (for knock-in only) and Sanger sequencing. All the knockout clones we acquired contain double knockouts of EWS/FLI1 and wild-type EWSR1, which shares the same N-terminus with EWS/FLI1 but does not maintain oncogenic transformation in A673 *(48)*. For further studies, we chose a knock-in clone that expresses tagged EWS/FLI1 at a level similar to the endogenous untagged EWS/FLI1 in wild-type A673, and a knockout clone that has relatively high transfection efficiency in preparation of samples for live-cell single-molecule imaging (Fig. 5D-F). Sequences for primers and sgRNAs are provided in Table S3. All plasmids used in this study, including the ones for genome-editing and transient transfections, are available upon request.

Antibodies

The following antibodies were used for western blots: anti-FLI1 (Abcam, ab133485), anti-EWSR1 (Abcam, ab133288) and anti-β-Actin (Sigma, A2228). The following antibodies were used for immunofluorescence: anti-EWSR1 (Abcam, ab54708) and donkey anti-Mouse secondary antibody, Alexa Fluor 647 (ThermoFisher Scientific, A-31571).

Luciferase assay

The firefly luciferase reporter contains a 500-bp promoter region (-1.6 kb to -1.1 kb) from the endogenous human *NR0B1* gene upstream of a minimal SV40 promoter *(33)* (precious gift from Stephen Lessnick). The 500-bp promoter region contains a 23x GGAA microsatellite. We co-transfected 293T cells with the firefly reporter, pRL-TK *Renilla* reporter plasmid and the relevant transcription factor (TF) cDNA plasmid (or an empty vector with an identical backbone as a control), and then measured the firefly and *Renilla* luciferase activity with the Dual-Luciferase® Reporter Assay System (Promega, E1960) following the manufacturer's instructions. The firefly luciferase activity was normalized to the *Renilla* luciferase activity to control for transfection efficiency. The relative firefly luciferase activity reflects transactivation capacity of the tested TF at the GGAA-microsatellite-driven promoter. Five (for Fig. 5G) or three (for Fig. S6C) independent replicates were performed for each condition. We did not detect the firefly luciferase activity using EWS/FLI1 cDNA and a control reporter vector (pGL3-Promoter) where luciferase expression is driven by the sole SV40 promoter (Fig. 5G, S6C), which confirms the essential role of GGAA-TF interaction in transactivation.

RT-qPCR and analyses

Total RNA was purified from cells using Trizol (ThermoFisher Scientific, 15596026) and quantified by Nanodrop. 500 ng of total RNA was retrotranscribed to cDNA using Maxima First Strand cDNA Synthesis Kit for RT-qPCR, with dsDNase (ThermoFisher Scientific, K1671). 5 µl of 1:20 cDNA dilutions were used for quantitative PCR with SYBR Select Master Mix for CFX (Applied Biosystems, ThermoFisher) on a BIO-RAD CFX Real-time PCR system. Five

independent replicates were performed for each gene. To normalize the data, we used the average value of 5 invariant transcripts (*GAPDH, MED12, NAE1, TUBULIN, BGALT3*) and calculated the normalized fold change for each target gene. Primers used are listed in Table S4.

Soft agar colony formation assay

To examine the malignant transformation capacity of endogenous EWS/FLI1-Halo, we seeded wild-type, EWS/FLI1 knockout, or EWS/FLI1-Halo knock-in A673 cells at a density of 5 x 10^4 per well in a 6-well plate in 0.4% SeaPlaque GTG agarose (Fisher, BMA50111) and IMDM (ThermoFisher, 12200036) medium containing 20% FBS and 1% penicillin-streptomycin, cultured the cells in agar at 37°C with 5% CO_2 for 15 days, and then stained the cells by applying to each well 200 µl of 1 mg/ml nitro blue tetrazolium chloride (NBT, ThermoFisher, N6495) in PBS. After culturing the stained cells in agar for 24 hours, we took images of the wells with a ChemiDoc MP imaging system (Bio-Rad). The live colonies appear as distinct dots on agar (Fig. S6D). We counted the number of sizable colonies (diameter > 70 µm) for quantitative analyses. To examine the transformation function of EWS(YS)/FLI1, the protocol was identical except that wild-type A673, EWS/FLI1 knockout A673 or EWS/FLI1 knockout A673 expressing exogenous EWS(YS)/FLI1 were seeded at a density of 1.5 x 10^4 per well in a 12-well plate (Fig. S10B), and stained with NBT 10 days after seeding. Three independent replicates were performed for each condition in Fig. S6D and S10B.

Fluorescence correlation spectroscopy (FCS) and analyses

Cells transfected with a fluorescent protein construct were plated on high-tolerance 150 µm glass coverslips (Marienfeld) and imaged at a single point with a Zeiss LSM880-NLO AxioExaminer microscope equipped with a 40x/1.2 W Korr M27 objective. Autocorrelation functions (ACFs) were computed with the Zen software. The autocorrelation function at a delay time of zero is equal to the inverse mean number of diffusing fluorescent particles in the observation volume under the condition that fluctuations in the intensity are due only to diffusing fluorophores *(18, 19)*. ACFs were first manually examined for two criteria: (1) absence of additional sources of fluctuations at small time delays (*e.g.* shot noise and triplet-singlet reactions), and (2) a constant mean fluorescent intensity in time, indicating an absence of photobleaching. ACFs out of compliance with these criteria were discarded. Estimates of the mean number of molecules in the observation volume were compared with a standard curve of purified fluorescent proteins to determine the concentration of fluorophores in the nucleoplasm. To measure the concentration of endogenous EWS/FLI1-Halo in A673 cells, we labeled the cells with 200 nM Halo ligand JF549 and used a standard curve of free JF549 in cell culture medium.

Due to the high density of fluorophores and internal heterogeneity of fluorescent proteins at the LacO array, ACFs cannot reliably be acquired within the array. Instead, to estimate the number of fluorophores at the LacO array, we first acquired an ACF in the nucleoplasm (outside any puncta) of LacO-containing U2OS cells transfected with the fluorescent protein of interest, then a z-stack of images through the cell (0.5 µm per step, 31 steps). The intensity within LacO arrays was then integrated and compared with the integrated intensity at an identically sized volume in the nucleoplasm to estimate the number of fluorophores inside the LacO array.

Fluorescence recovery after photobleaching (FRAP) and analyses

FRAP was performed on an inverted laser scanning confocal microscope (Zeiss, LSM 710 AxioObserver) equipped with 34-channel spectral detection, a motorized stage, a full incubation chamber maintaining 37°C and 5% CO_2, a heated stage, an X-Cite 120 illumination source as well as several laser lines (405, 458, 488, 514, 561, 591, 633 nm). The 561 nm laser and the epi-illumination mode were used for FRAP measurements. Images were acquired with a 40x Plan NeoFluar NA1.3 oil-immersion objective under control of the Zeiss Zen software.

To measure the FRAP dynamics of mCherry-labeled LCD-LacI or LacI at the LacO array (Fig. 1E, S3), we acquired 500 frames at one frame per 1.5 seconds with the first 3 frames acquired before the bleach pulse for the measurement of baseline fluorescence of the bleach spot and the whole nucleus. We chose to photobleach a circular spot (radius ranging from 0.6 to 2 μm) that just covered the LacO-associated hub using the 561 nm laser at maximum intensity. To measure the FRAP dynamics of JF549-labeled endogenous or transiently expressed EWS/FLI1-Halo (Fig. S8C), we acquired 1000 frames at one frame per 0.3 second with the first 5 frames acquired before the bleach pulse. A circular bleach spot (radius ~0.7 μm) was chosen in a region with homogenous fluorescence and at least 1 μm from nuclear or nucleolar boundaries.

To correct for xy-drift of the bleached spot due to live cell movement during movie acquisition, we used a published ImageJ plugin "Template Matching and Slice Alignment" (https://sites.google.com/site/qingzongtseng/template-matching-ij-plugin#description). Then we used three steps of normalization to quantify the FRAP signal in the bleach spot. First, we normalized the mean intensity of the bleach spot and the whole nucleus at time t to the respective pre-bleaching baseline intensity, *i.e.,* $I_{frap}(t)/I_{frap\text{-}pre}$ and $I_{whole}(t)/I_{whole\text{-}pre}$. Secondly, we normalized the relative bleach spot intensity to the relative nuclear intensity by

$$I_{frap\text{-}2norm}(t) = (I_{frap}(t)/I_{frap\text{-}pre})/(I_{whole}(t)/I_{whole\text{-}pre}). \qquad (1)$$

Then we calculated the bleach depth (ΔI_{frap}), *i.e.*, the difference between the double-normalized FRAP intensity before and at the first frame (t_1) after bleach pulse by

$$\Delta I_{frap} = 1\text{-}I_{frap\text{-}2norm}(t_1). \qquad (2)$$

Finally, we normalized the bleach depth to 100%, and the triple-normalized FRAP intensity became

$$I_{frap\text{-}3norm}(t) = 1\text{-}(1\text{-}\ I_{frap\text{-}2norm}(t))/\Delta I_{frap}\ . \qquad (3)$$

For each experiment, we averaged the drift-corrected and normalized FRAP curves from multiple single cells to generate a mean FRAP curve. In order to choose an appropriate model to fit the FRAP dynamics of LacO-associated hubs, we ensured that the FRAP dynamics of mCherry-TAF15 LCD-LacI or mCherry-LacI at the LacO array were independent of the bleach spot size (Fig. S3A-B), suggesting that the observed FRAP dynamics are independent of diffusion *(20, 26)*. We found the FRAP dynamics are best fitted with the reaction-dominant two-binding-state model below

$$I_{frap\text{-}3norm}(t) = 1\text{-}Ae^{-k1t}\text{-}Be^{-k2t}, \qquad (4)$$

where k_1 and k_2 are fast and slow dissociation rate constants, respectively. A single exponential

equation does not fit the FRAP traces well as the one-binding-state model does not properly describe the FRAP dynamics here that involve two binding states (data not shown). After model fitting, we used the slow dissociation rate constant for further analyses on how LCD changes the dynamics of LacI-LacO specific interaction, as the fast dissociation process in the FRAP dynamics likely reflects nonspecific LacI-chromatin interactions.

Live-cell imaging of LCD hubs during hexanediol treatments

On the previously described confocal microscope with the incubation chamber maintaining 37°C and 5% CO_2, live LacO-array-containing U2OS cells expressing EYFP-labeled Sp1 LCD-LacI or FUS LCD-LacI were imaged under epi-illumination using the 514 nm laser with a frame acquisition time of 1.938 sec except where otherwise noted.

We prepared fresh stock solutions of 1,6-hexanediol (Aldrich, 240117) or 2,5-hexanediol (Aldrich, H11904) with different m/v concentrations (20%, 10% or 4%) in the phenol-red-free medium for live-cell imaging. Before starting with image acquisition, we had 1 ml of phenol-red-free medium in the 35 mm dish. Without pausing imaging of LCD hubs, we added 1 ml of the pre-warmed hexanediol stock solution to the dish to reach a final concentration of 10%, 5% or 2%. The time of hexanediol addition was the time "0" in Fig. 2C-D and S5C-D. The number of intra-nuclear puncta was quantified using the "Find Maxima" function of ImageJ *(49)*.

3D DNA Fluorescence in situ hybridization (FISH)

We followed the published 3D DNA FISH protocol *(22, 50)* except that the EWS/FLI1-Halo knock-in A673 cells were labeled with the JF549 HaloTag ligand before fixation. The DNA FISH probes were prepared by incorporating Red 650 dUTP (enhanced Cy5, Enzo, ENZ-42522) into relevant bacterial artificial chromosome (BAC) DNA with the Nick Translation DNA Labeling System (Enzo, ENZ-42910) according to the manufacturer's instructions. The following BAC clones (purchased from BACPAC Resources Center at Children's Hospital Oakland Research Institute) were used for generating locus-specific FISH probes: RP11-426N1 (for *CAV1*), RP11-622M2 (for *FCGRT*), RP11-467M9 (for *ABHD6*), RP11-711N9 (for *KDSR*), RP11-66P3 (for *KIAA1797*), RP11-431J16 (for non-GGAA 1, detecting *ADGRA3*), RP11-248F15 (for non-GGAA 2, detecting *REEP5*). Ultrapure, genomic DNA-free BACs were extracted with QIAGEN Large-Construct Kit (QIAGEN, 12462) before used as the template DNA in nick translation reactions.

Confocal fluorescence imaging and analyses

Z stacks of fixed cell samples were acquired on the previously described confocal microscope with a pinhole size of 1 airy unit and a slice interval of 0.4 μm. We used 488 nm, 514 nm and 561 nm lasers to excite fluorescence of JF500-labeled Halo-RPB1 (JF500 λ_{max}=500 nm, λ_{em}=524 nm, ε_{500}=60,760 M^{-1} cm^{-1}), EYFP-LCD-LacI and mCherry-LCD respectively, which were expressed solely or in combination in LacO-containing U2OS cells. We used 561 nm and 633 nm lasers to excite fluorescence of JF549-labeled EWS/FLI1-Halo and Red 650 dUTP-labeled DNA FISH in knock-in A673 respectively. Before acquiring all the fluorescence images, we carefully set the laser intensity and microscope detectors to make sure that no pixel in the images

was saturated. For simultaneous 2-color imaging (Fig. 1F, 2A, 4D, 5C, S4, S5B, S9B), we used proper emission filters and ensured no bleed-through between the two channels by imaging fixed cell samples that contain either fluorophore under the same 2-color imaging settings.

To measure the nuclear fluorescence intensity of EYFP- or mCherry-labeled LCD-LacI or LacI alone in individual cells (Fig. 1C-D, S2), we included all the pixels of the cell nucleus, that is, the LacO-affiliated hub, puncta unaffiliated with the LacO array, and the low-intensity regions outside the hubs were all taken into account in the measurement. Then we calculated the mean nuclear TF concentration by comparing the fluorescence intensity with the standard curves (Fig. S1B-C).

Figure S5A illustrates the way we quantified enrichment of mCherry-LCD at LacO arrays bound by EYFP-LCD-LacI (Fig. 2B, S9A, C-D). First, we selected the slice (#N) in the EYFP-channel z stack where the LacO-associated hub was brightest, manually located the LacO array center in the cell nucleus and plotted the radial profiles surrounding this center pixel in both the EYFP image and slice #N in the mCherry-channel z stack. The EYFP intensity radial profile allows us to locate the concentration peak and periphery of the LacO-associated hub. Next, from the mCherry intensity radial profile, we extracted the intensity at the peak location (I_{peak}) and averaged two intensity values immediately outside the periphery location with an interval ranging from 0.23 to 0.45 μm ($I_{periphery}$). Finally, we calculated the peak to periphery intensity ratio ($I_{peak}/I_{periphery}$) as a measure of mCherry-LCD enrichment at the LacO array. A ratio above 1 suggests LCD-LCD interactions.

To quantify enrichment of JF500-labeled Halo-RPB1 at the LacO array bound by mCherry-FET LCD-LacI or mCherry-LacI, we first selected the slices in the mCherry-channel z stack that covered ~80% of the intensity of a LacO-associated hub, averaged these slices as well as the corresponding JF500 slices, and located the LacO array center pixel in the average mCherry image. Then we cropped a square region (8.30 μm x 8.30 μm) in the average mCherry and JF500 images centering the LacO array center pixel. We processed tens of LacO arrays following the above procedure, averaged the cropped square images in both channels (Fig. 1G, left), and plotted the average radial profile of JF500 intensity surrounding the center pixel (Fig. S4B). To acquire the baseline radial profile of JF500 intensity in the nucleus outside the LacO array, we manually selected 10 non-LacO pixels from each cell nucleus in the average mCherry image, each pixel being away from nuclear or nucleolar boundaries with distances comparable to the distances between the LacO array center and the boundaries. Then we plotted the radial profiles of JF500 intensity surrounding these pixels in all the cell nuclei under analyses and calculated the average radial profile. Subtracting this baseline radial profile from the radial profile at LacO array resulted in the background-free radial profile of Halo-RPB1 (Fig. S4C). We compared the mean Halo-RPB1 (Pol II) intensity values at the center of the LacO array (first points on the background-free radial profiles in Fig. S4C) bound by mCherry-labeled FET LCD-LacI or LacI alone in Fig. 1G (bar plot on the right). To calculate the error bar for each condition in Fig. 1G, we used the bootstrap method *(45)* to generate 2000 resampled image sets from the original set of JF500 (Halo-RPB1) images centering the LacO array, calculated the mean Halo-RPB1 intensity at LacO array center of each image set and then the standard deviation of the mean values. We also took the bootstrapped mean value as the test statistic and performed two-sample t-test to calculate p-values.

The procedure we used to evaluate enrichment of JF549-labeled EWS/FLI1-Halo at specific genes visualized by DNA FISH (Fig. 4D-E) was similar except that the cropped square regions were slightly larger (8.51 μm x 8.51 μm), images of more loci (~1000) were processed for each gene and fewer non-FISH-puncta pixels (2 to 4 per cell nucleus) were manually selected for measurement of baseline JF549 intensity. From the DNA FISH and JF549 images, we cropped square regions centering all the FISH puncta (Fig. 4D) or non-FISH-puncta pixels, averaged them respectively, and got a two-color FISH puncta image or baseline image (averaged from non-FISH-puncta square regions). Subtracting the baseline image from the FISH puncta image resulted in the averaged background-free two-color image of FISH puncta and EWS/FLI1-Halo (Fig. 4E).

Lattice light sheet microscopy

The image volumes of EWS/FLI1 hubs were generated by the lattice light sheet (LLS) microscope *(21)*. Each image volume includes 100 image frames, which were acquired at 10 ms exposure time with minimal photobleaching. The collected data have spatial resolution of 230 nm in XY and 370 nm in Z.

In preparation of experiments, LLS scope was aligned and the imaging chamber with heating block was preheated to 37°C. A673 cells were seeded on 5 mm coverslips (Warner Instruments) and placed into the imaging chamber. The samples were then imaged on the LLS scope using Bessel beams arranged in a square lattice configuration in dithered mode *(21)*. Live cells immersed into imaging medium were imaged by exciting each plane with a 560 nm laser at ~10 μW (at the rear aperture of the excitation objective) for 10 ms. The fluorescence generated within the specimen was collected by a detection objective (CFI Apo LWD 25XW, 1.1 NA, Nikon), filtered through a 440/521/607/700 nm BrightLine quad-band bandpass filter (Semrock), and eventually recorded by an ORCA-Flash 4.0 sCMOS camera (Hamamatsu). The cells were imaged by sample scanning mode and the dithered light sheet at 300 nm step size, thereby capturing a volume of ~25 μm x 51 μm x 30 μm (corresponding to 500 × 512 × 100 pixels in deskewed data). The generated raw images were deskewed and then deconvoluted by running 8 Richardson-Lucy iterations.

Single-particle tracking (SPT) and analyses

Single-molecule imaging for Halo-tagged EWS/FLI1 variants (wild-type, EWS(YS)/FLI1, FLI1 DBD) was conducted on a custom-built Nikon (Nikon Instruments Inc.) TI microscope described in detail in *(24)*. Single-molecule imaging of various Halo-tagged LCDs was conducted on another Nikon microscope with the same equipment except a LUNV laser unit with alignment-free monolithic optical based beam combiner and AOTF modulation, providing guaranteed output powers at the following 4 wavelengths with 2 single mode optical fiber outputs: 405 nm (20 mW), 488 nm (70 mW), 561 nm (70 mW), and 647 nm (125 mW). Motorized ND filters were installed on all laser lines. We took images with a 100x/NA 1.49 oil-immersion TIRF objective (Nikon apochromat CFI Apo TIRF 100x Oil) under highly inclined and laminated optical sheet (HILO) illumination *(51)* using following laser lines: 488 nm for EYFP; 561 nm for JF549; 405 nm and 633 nm or 647 nm for photo-activation and illumination of PA-JF646, respectively. The incubation chamber maintained a humidified 37°C atmosphere with 5% CO_2

and the objective was similarly heated to 37°C for live-cell experiments.

To measure the residence times (RTs) of endogenous EWS/FLI1-Halo in and outside its hubs, we labeled knock-in A673 cells with 200 nM JF549 and 20 nM PA-JF646. High-concentration JF549 labeling allows visualization of EWS/FLI1 hubs, whereas low-concentration PA-JF646 labeling allows real-time tracking of individual EWS/FLI1 molecules. We kept the intensity of the 405 nm laser low enough that it only photo-activated a handful of PA-JF646-labeled EWS/FLI1-Halo molecules at a time in the nucleus. Using a long image acquisition time (500 ms), we blurred out fast moving molecules into the background and visualized individual stable EWS/FLI1 binding events *(23)*(Movie S3). To minimize photobleaching of dyes, we took time-lapse images (500 ms image acquisition time) in the JF549 channel with a 10 sec interval, and continuously acquire images in the PA-JF646 channel with constant low-intensity excitation at 633 nm.

All the single-molecule images taken in the PA-JF646 channel were processed using a custom-written MATLAB implementation of the MTT algorithm *(52)*. A GUI of this implementation, SLIMfast *(53)*, is available in the supplemental materials of *(54)*. Briefly, single molecules are localized using 2-dimensional Gaussian fitting (approximating the microscope PSF) subject to a generalized log-likelihood ratio test with a 'localization error' threshold (in the range of 10^{-6}-10^{-7}), with the option of allowing deflation to detect molecules partially obscured by others. Tracking, that is connecting localizations between consecutive frames, was limited by setting a maximal expected diffusion constant, and takes the trajectory history into account as well as allowing for gaps due to blinking or missed localizations. We used the following algorithm parameters for SPT: localization error: 10^{-7}; deflation loops: 3; blinking (frames): 2; maximum number of competitors: 1; maximal expected diffusion constant ($\mu m^2/s$): 0.1. Thousands of single-molecule trajectories were recorded in each cell.

We processed the JF549 images using a custom-written Macro program in ImageJ, which defined the EWS/FLI1-Halo hubs as intra-nuclear regions above a fluorescence intensity threshold, assigned pixel values of in- and outside-hub regions as 1 and 0 respectively, and therefore generated a dynamic mask of hubs. Of note, both false positives and false negatives inevitably existed in mask generation as 1) the HILO illumination was not perfectly homogeneous across the cell nucleus; 2) JF549 slowly photobleached during movie acquisition; 3) hubs were small, crowded, surrounded by significant fluorescence background, and slowly moved in and out of the focus; and 4) one intensity threshold was used for hub definition throughout the movie. Using a custom-written Matlab program, we separated all the single-molecule trajectories from a cell into in- and outside-hub groups based on the fraction of lifetime (F) a molecule located in the "hub region". We found the average in-hub lifetime fraction (F_{ave}) of all the trajectories in a cell was in the range of 20~30%. Thus we used the following trajectory sorting standard in calculating EWS/FLI1-Halo RTs presented in this study: $F > 50\%$ for in-hubs and $F < 5\%$ for outside-hubs. We also tried alternative sorting standard: $F > (2F_{ave}\text{-}10\%)$ for in-hubs and $F < 10\%$ for outside-hubs, which resulted in slightly different absolute in- and outside-hub RTs of EWS/FLI1-Halo but did not affect our conclusions. We did not use stringent standards like $F = 1$ or $F > 0$ for in-hub molecule definition due to errors in hub detection throughout the movie acquisition.

After sorting, we recorded the lengths of trajectories in either group and used them to generate

a survival probability (1-CDF) (Fig. S8B). Then we fitted the survival probability curve to a two-term exponential model below and extracted RTs of EWS/FLI1-Halo corresponding to specific and nonspecific binding (Fig. S8A) *(23, 24, 55)*

$$P(t) = Ae^{-k1t-}+(1-A)e^{-k2t}, \quad (5)$$

$$1/k_1 = \tau_{ns}, \; 1/k_2 = \tau_s,$$

where τ_s and τ_{ns} are specific and nonspecific RTs, respectively. We only focused on the specific RT.

To correct for dye photobleaching and axial cell or chromatin drift *(24)*, we measured the specific RT (τ_{H2B}) of histone H2B (largely immobile on chromatin) by performing SPT of PA-JF646-labeled H2B-Halo that was stably expressed in A673 cells under identical illumination intensity and image acquisition settings (Fig. S8B). Then we corrected the specific RT of EWS/FLI1-Halo by following equation and used the corrected RT for further analyses.

$$\tau_{corrected} = 1/(1/\tau_s - 1/\tau_{H2B}), \quad (6)$$

We recorded 20 min movies from at least 6 EWS/FLI1-Halo knock-in and 4 H2B-Halo A673 cells per day, conducted at least 3 independent experiments on different days and presented the average corrected RT.

We performed FRAP of JF549-labeled EWS/FLI1-Halo in the knock-in A673 cells (Fig. S8C), fitted the FRAP curve with the two-binding-state model described above, and extracted the long-lived RT ($1/k_2$) of EWS/FLI1-Halo corresponding to slow dissociation to be 78 sec. The fact that the long-lived RT of EWS/FLI1-Halo measured by FRAP is close to the in-hub RT (90 sec) and overall RT (59 sec) measured by SPT cross-validates the two methods in measurement of specific RTs.

We followed the same procedure of 2-color single-molecule imaging acquisition and data analyses to measure the in-hub and outside-hub RTs of Halo-tagged EWS/FLI1 or its mutants (EWS(YS)/FLI1 or FLI1 DBD) that were transiently expressed in EWS/FLI1 knockout A673. To measure the RTs of Halo-tagged EWS or EWS(YS) LCD at EWS/FLI1-$SNAP_f$ hubs in the knockout A673 cells, we used the same procedure except that 1) a $SNAP_f$-tag ligand cp-JF549 (200 nM) was used to label EWS/FLI1-$SNAP_f$ instead for visualizing EWS/FLI1 hubs; 2) the JF549 channel acquired images continuously; and 3) SPT of PA-JF646-labeled Halo-LCDs was performed with low-intensity excitation at 647 nm instead of 633 nm.

To measure the RTs of various Halo-LCDs in U2OS cells at EYFP-labeled LCD hubs that were either LacO-array-associated or non-array-affiliated, the procedure was identical except that 1) the cells were only labeled with one HaloTag ligand, PA-JF646 (2 nM) for single-molecule imaging; 2) images of LCD hubs were continuously acquired in the EYFP channel with 488 nm laser excitation; 3) SPT of PA-JF646-Halo-LCDs was performed with 647 nm excitation; 4) U2OS cells stably expressing H2B-Halo were used for photobleaching correction; and 5) an in-hub Halo-LCD molecule was defined as that localized in a hub for more than once throughout its trajectory ($F > 0$). The reason for a different in-hub molecule definition here was that these LCD hubs were significantly brighter (relative to background intra-nuclear

fluorescence), larger, fewer and more sparsely distributed (Fig. 3A) than the EWS/FLI1 hubs in A673 (Fig. 4C), which led to much lower errors in hub detection.

Supplementary Text:

All the codes for imaging data analyses have been submitted to GitHub and are publicly available at https://github.com/Shasha-Chong/CodeFor2018SciencePaper.

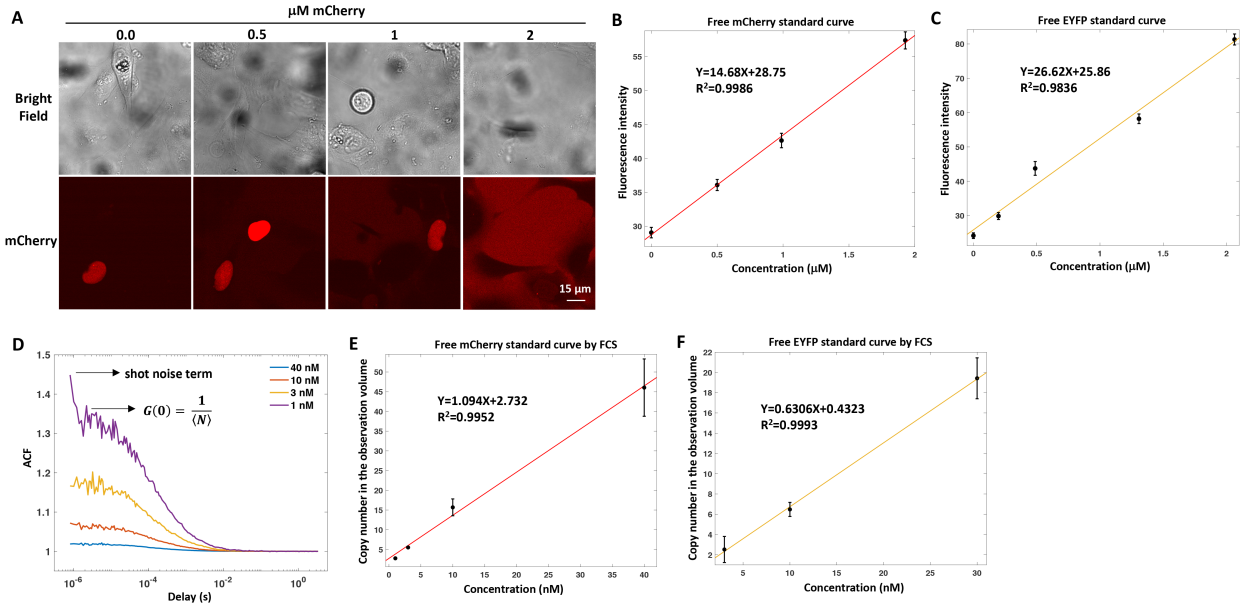

Fig. S1. Two methods to measure protein concentration in live cells.

(**A**) Bright field and confocal fluorescence images of live U2OS cells containing a LacO array (3, with ~40,000 LacO repeats and a single transcription unit) and transiently expressing mCherry-LacI. Purified mCherry was added to the imaging media, reaching the final concentration indicated above the images. The fluorescence intensities of free mCherry outside live cells were measured in three images to generate the standard concentration curve of mCherry.

(**B-C**) Fluorescence intensity as a function of free mCherry (**B**) or EYFP (**C**) concentration measured by the imaging method shown in (**A**). Error bars represent standard errors.

(**D**) FCS measurements of purified mCherry at known concentrations in the media used for live-cell imaging. The y-intercept of the ACF, G(0) (not considering shot noise), is used to estimate the inverse mean number of molecules (N) in the observation volume and generate the standard concentration curve for mCherry.

(**E-F**) Copy number in the observation volume as a function of free mCherry (**E**) or EYFP (**F**) concentration measured by FCS as shown in (**D**). Error bars represent standard deviations.

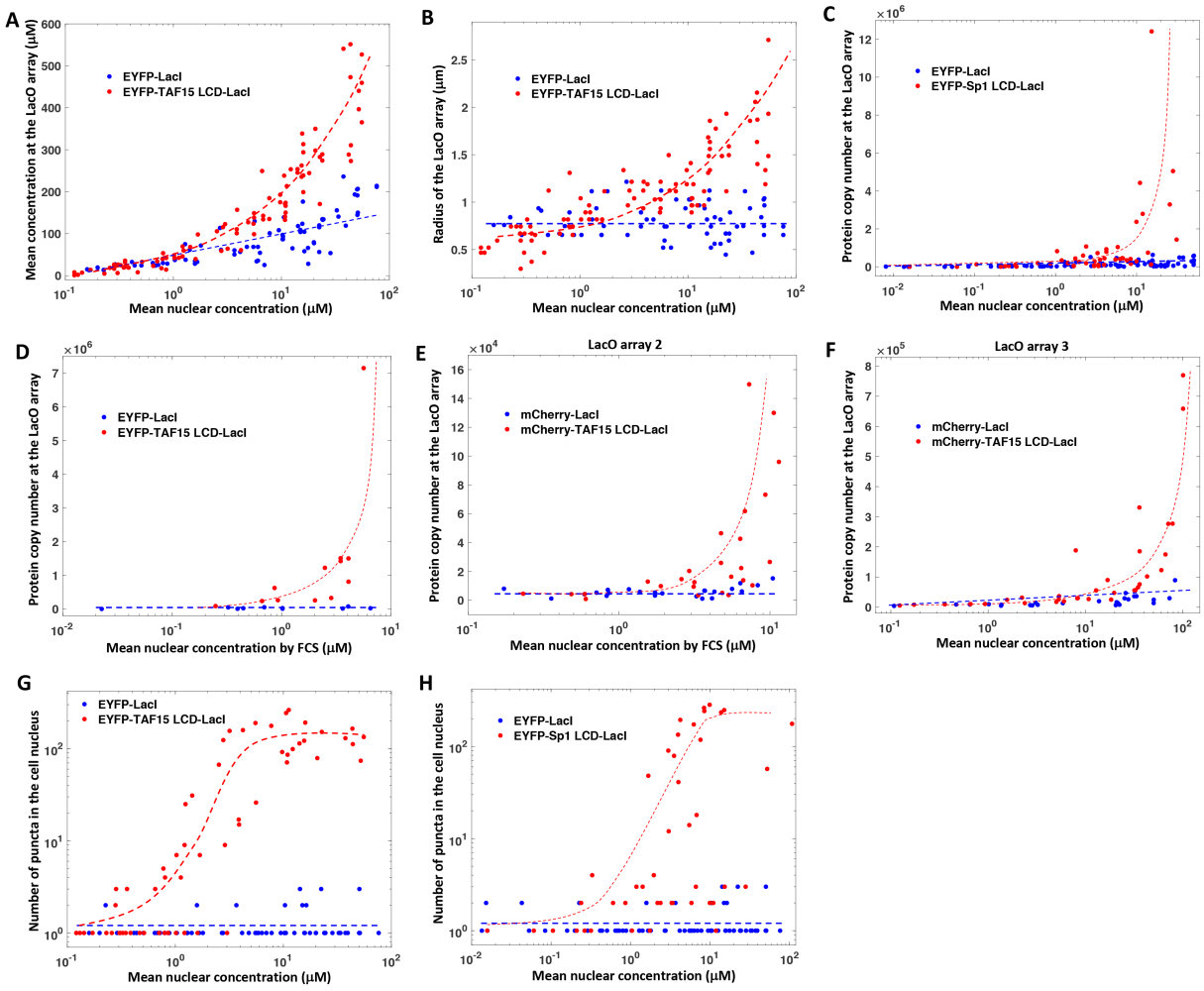

Fig. S2. LCD can form interaction hubs at the targeted LacO array or spontaneously as non-LacO-affiliated intranuclear puncta upon overexpression.

(**A**) Mean concentration of EYFP-labeled TAF15 LCD-LacI (red) or LacI (blue) at LacO array 1 (~50,000 LacO repeats) as a function of mean nuclear concentration of the TF. Each dot represents one cell.

(**B**) Radius of LacO array 1 bound by EYFP-labeled TAF15 LCD-LacI (red) or LacI (blue) as a function of mean nuclear concentration of the TF.

(**C**) Copy number of EYFP-labeled Sp1 LCD-LacI (red) or LacI (blue) molecules bound to LacO array 1 as a function of mean nuclear concentration of the TF. Concentrations and copy numbers in (**A**), (**B**) and (**C**) were measured by fluorescence intensity comparison.

(**D-E**) Copy number of EYFP-labeled (**D**) or mCherry-labeled (**E**) TAF15 LCD-LacI (red) or LacI (blue) molecules bound to LacO array 1 (**D**) or 2 (~15,000 LacO repeats) (**E**) as a function of mean nuclear concentration of the TF. Concentrations and copy numbers were measured by FCS. Each dot represents one cell.

(**F**) Copy number of mCherry-labeled TAF15 LCD-LacI (red) or LacI (blue) molecules bound to LacO array 3 (with ~ 40,000 LacO repeats and a single transcription unit) as a function of mean nuclear concentration of the TF. (**A**) to (**F**) suggest that a LacO array can accumulate more

copies of LCD-LacI than of LacI alone, thus the array can mediate formation of LCD hubs that involve extensive LCD self-interactions.
(**G-H**) Number of intranuclear puncta of EYFP-labeled TAF15 LCD-LacI (**G**) or Sp1 LCD-LacI (**H**) (red) compared with LacI (blue) as a function of mean nuclear concentration of the TF. TAF15 LCD-LacI and Sp1 LCD-LacI, but not LacI alone, can self-aggregate at high expression levels. Concentrations and copy numbers in (**F**), (**G**) and (**H**) were measured by TF concentration measured by fluorescence intensity comparison.

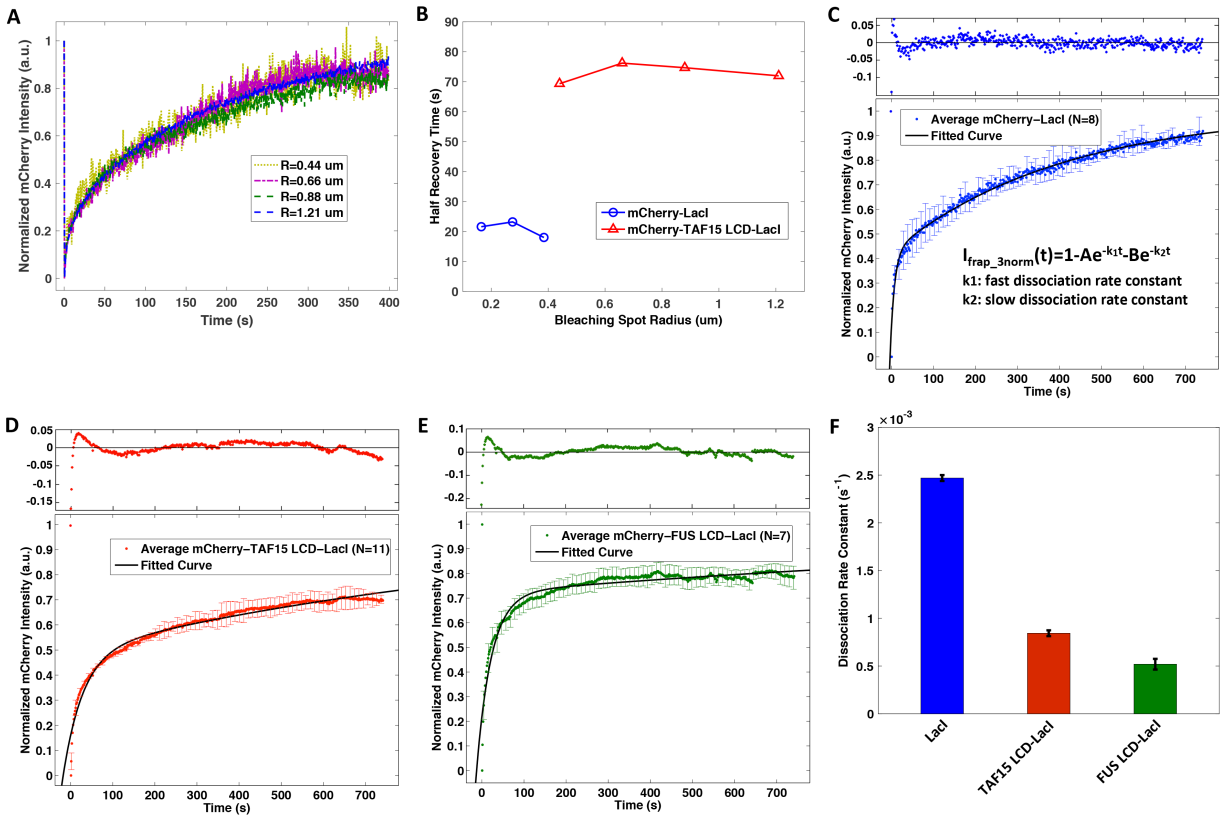

Fig. S3. The formation of an LCD interaction hub slows down the dissociation of LCD-LacI from the LacO array according to FRAP.

(**A**) FRAP curves at the LacO array 1 (~50,000 LacO repeats) bound by mCherry-TAF15 LCD-LacI in one U2OS cell with different photobleaching spot radii (R). The FRAP dynamics are independent of the radius.

(**B**) Half life ($\tau_{1/2}$) of FRAP at the LacO array 1 bound by mCherry-LacI (blue) or mCherry-TAF15 LCD-LacI (red) as a function of the photobleaching spot radius in one U2OS cell. $\tau_{1/2}$ is independent of the radius. (**A**) and (**B**) both suggest that FRAP dynamics at the LacO array is reaction-dominant.

(**C-E**) Averaged FRAP curve at LacO array 1 bound by mCherry-labeled LacI (**C**, blue), TAF15 LCD-LacI (**D**, red) or FUS LCD-LacI (**E**, green) fitted with a reaction-dominant two-binding-state model (fitted curves in black, model shown by the inner equation in **C**). The slow dissociation rate constants reflect specific LacI-LacO interaction dynamics. Error bars represent standard deviations. Top panels show the residuals from the fitted model.

(**F**) Slow (k2) dissociation rate constants of mCherry-labeled LacI (blue), TAF15 LCD-LacI (red) or FUS-LacI (green) at LacO array 1 extracted from the two-binding-state model. Fusing an LCD to LacI significantly reduces the dissociation rate. Error bars represent 95% confidence bounds for the fitted dissociation rate constants.

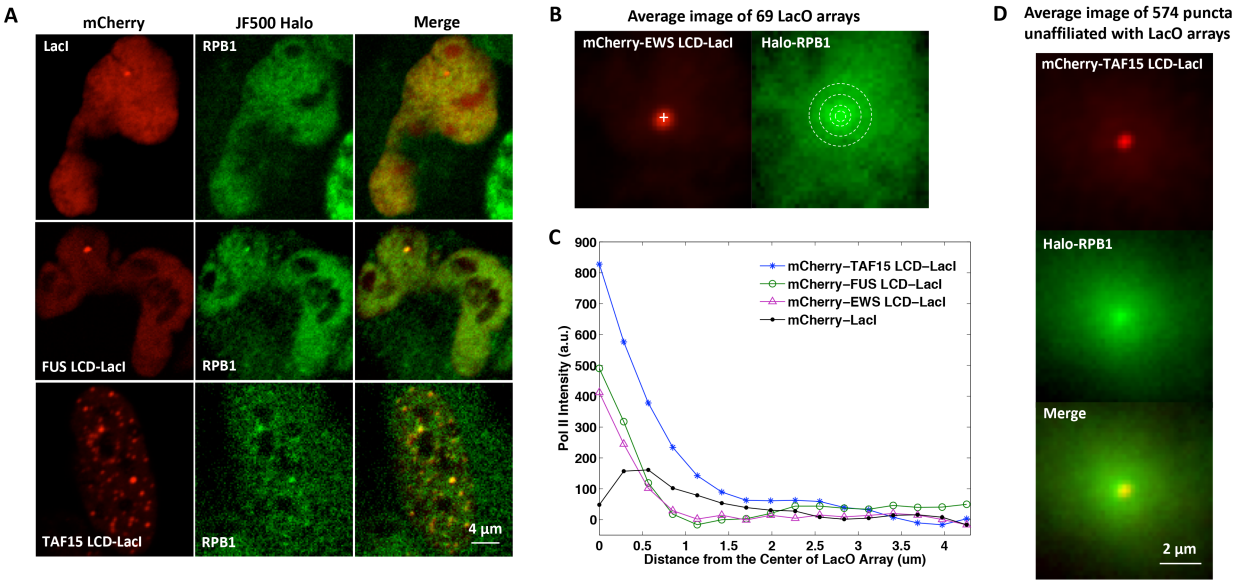

Fig. S4. LacO-array-associated LCD hubs recruit RNA Pol II.
(**A**) Confocal fluorescence images show that Halo-RPB1 (labeled with HaloTag ligand JF500 at 200 nM, green) is enriched at LacO array 2 (~15,000 LacO repeats) bound by mCherry-labeled FUS LCD-LacI or TAF15 LCD-LacI, but not LacI (red).
(**B**) Averaged Halo-RPB1 image at LacO array 2 bound by mCherry-EWS LCD-LacI (N=69). The radial profile of Halo-RPB1 is plotted centering the LacO array as marked on the images.
(**C**) Average background-free radial profile of Halo-RPB1 (Pol II) at LacO array 2 bound by mCherry-labeled TAF15 LCD-LacI (blue), FUS LCD-LacI (green), EWS LCD-LacI (magenta), or LacI (black). FET LCD-LacI enriches Pol II at the LacO array while LacI does not.
(**D**) Averaged image of Halo-RPB1 (labeled with HaloTag ligand JF500 at 200 nM, green) at mCherry-TAF15 LCD-LacI (red) puncta unaffiliated with LacO arrays (N=574 from 5 cells).

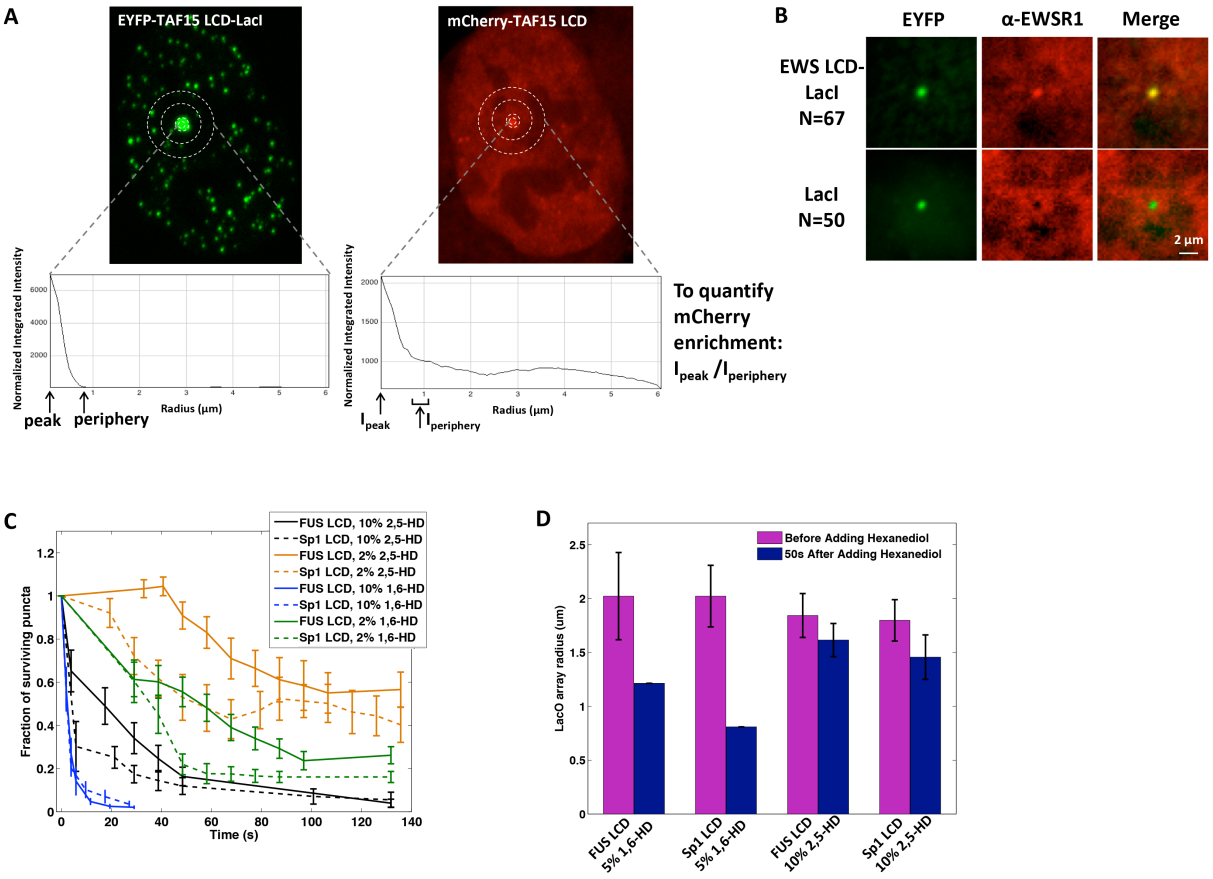

Fig. S5. Assays for studying selective protein-protein interactions involved in LCD hub formation.

(**A**) Representative images to illustrate quantification of mCherry-LCD at the LacO array bound by EYFP-LCD-LacI. We first located the center of LacO array in the cell nucleus according to the EYFP channel image (upper left) and plotted radial profiles surrounding the center pixel in both EYFP and mCherry channel images (lower). The EYFP intensity radial profile allows us to locate the concentration peak and periphery of LacO-associated LCD hubs (lower left). Next, from the mCherry intensity radial profile (lower right), we extracted the intensity at the peak location (I_{peak}) and immediately outside the periphery location ($I_{periphery}$, averaged from two adjacent points in the radial profile, each representing the average intensity in a 0.25-μm-thick circular ring area), and calculated the peak to periphery intensity ratio ($I_{peak}/I_{periphery}$) as the measure of mCherry-LCD enrichment at the LacO array. A ratio above 1 suggests LCD-LCD interactions.

(**B**) Averaged EWSR1 immunofluorescence images shows the endogenous EWSR1 (red) is enriched at LacO array 1 (~50,000 LacO repeats) bound by EYFP-labeled EWS LCD-LacI but not LacI (green). The anti-EWSR1 antibody does not target EWS LCD. Possibly due to difficulty in antibody penetration into the dense LacO array region in the absence of specific interactions, we even detected depletion of anti-EWSR1 antibody at the LacO arrays bound by LacI only (lower middle). This result confirms that LacO-associated LCD hubs interact with not only overexpressed but also endogenous LCDs.

(**C**) Number of nuclear puncta formed by FUS (solid lines) or Sp1 (dashed lines) LCD surviving over time upon addition of 1,6-HD or 2,5-HD at different concentrations. 2,5-HD melts self-

aggregated LCD hubs more slowly and less thoroughly than 1,6-HD at the same concentration. Error bars represent standard errors.
(**D**) Due to disruption of LacO-array-associated LCD hubs, the apparent radius of the array bound by EYFP-LCD-LacI decreases upon addition of HDs. The effect of 1,6-HD is more significant than 2,5-HD. Error bars represent standard errors.

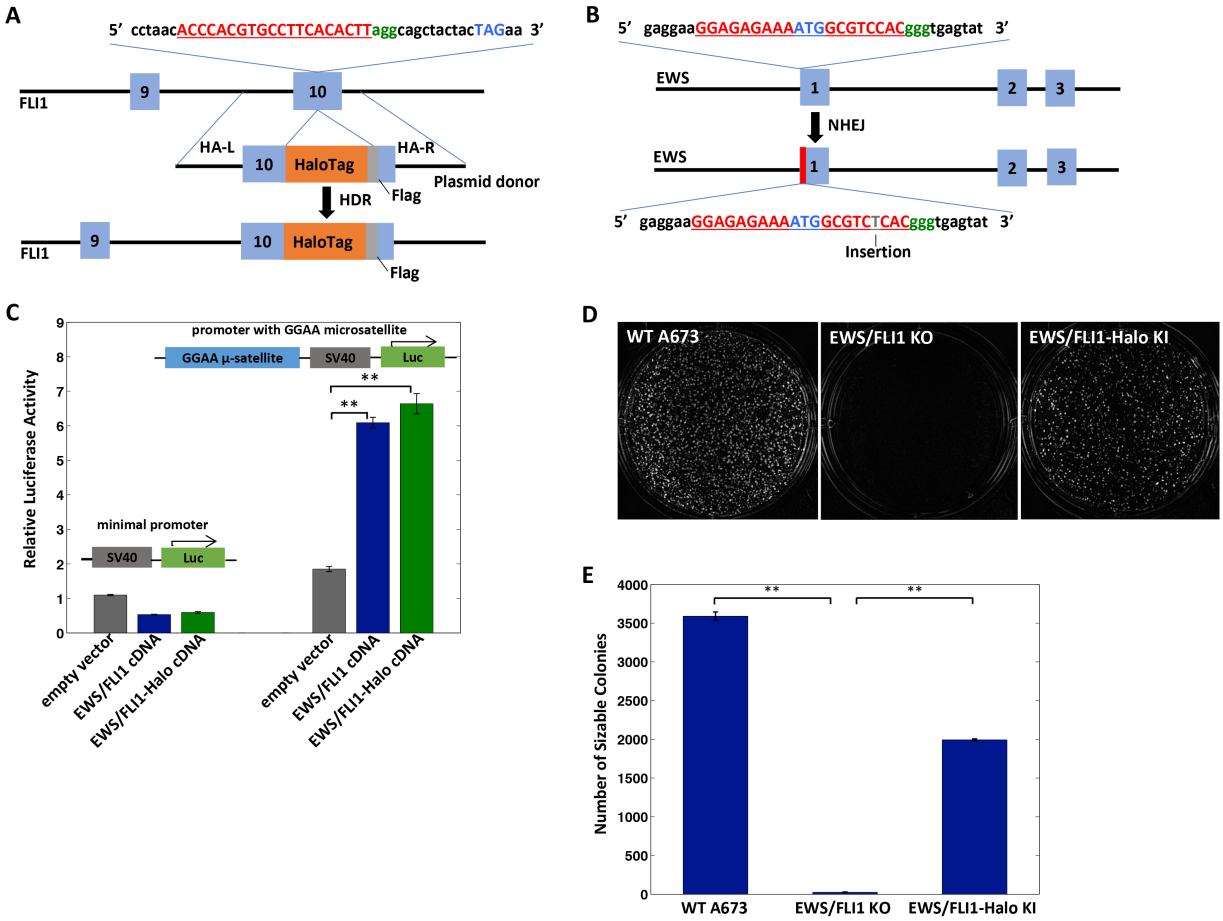

Fig. S6. Genome editing of A673 cells

(**A-B**) Schematics for genome editing of A673 cells to generate EWS/FLI1-Halo knock-in and EWS/FLI1 knockout lines. We used a single-guide RNA (sgRNA, underlined red sequence) targeting the genomic sequence near the FLI1 stop codon (blue TAG) for the knock-in (A), and an sgRNA targeting the EWS start codon (underlined blue ATG) for the knockout (B). PAM sequences are in green. RNA-guided Cas9 generates a double-strand break at the targeted genomic loci. In the presence of a donor plasmid that contains the HaloTag and Flag-tag coding sequences followed by a stop codon and flanked by two homology arms (HA-L and HA-R), The break can be repaired by the homology directed repair (HDR) pathway to incorporate the HaloTag to the C-terminus of FLI1 *(33)*(**A**). On the other hand, in the absence of a donor plasmid, the break is repaired through non-homologous end joining (NHEJ) *(36)*, which can create indels (a T insertion in this case) near the start codon of EWS that inhibits expression of EWS/FLI1 (**B**).

(**C**) Luciferase assay using a reporter construct that contains a GGAA microsatellite upstream of a minimal SV40 promoter. EWS/FLI1-Halo activates the reporter as efficiently as the wild-type EWS/FLI1. **: statistically significant difference of pairwise comparisons ($p < 0.01$, two-sample t-test). Error bars represent standard errors ($n = 3$).

(**D**) Soft agar colony formation assay to examine the cancerous transformation capacity of modified A673 cell lines. EWS/FLI1-Halo knockin (KI) A673 cells are able to form colonies in agar similar to wild-type (WT) A673, albeit with lower efficiency. In contrast, as expected the EWS/FLI1 knockout (KO) A673 cells do not grow in agar.

(**E**) Number of sizable colonies (diameter > 70 μm) formed by WT, EWS/FLI1 KO and EWS/FLI1-Halo KI A673 cells in soft agar, quantified from (D). **: $p < 0.01$, two-sample t-test. Error bars represent standard errors (n = 3).

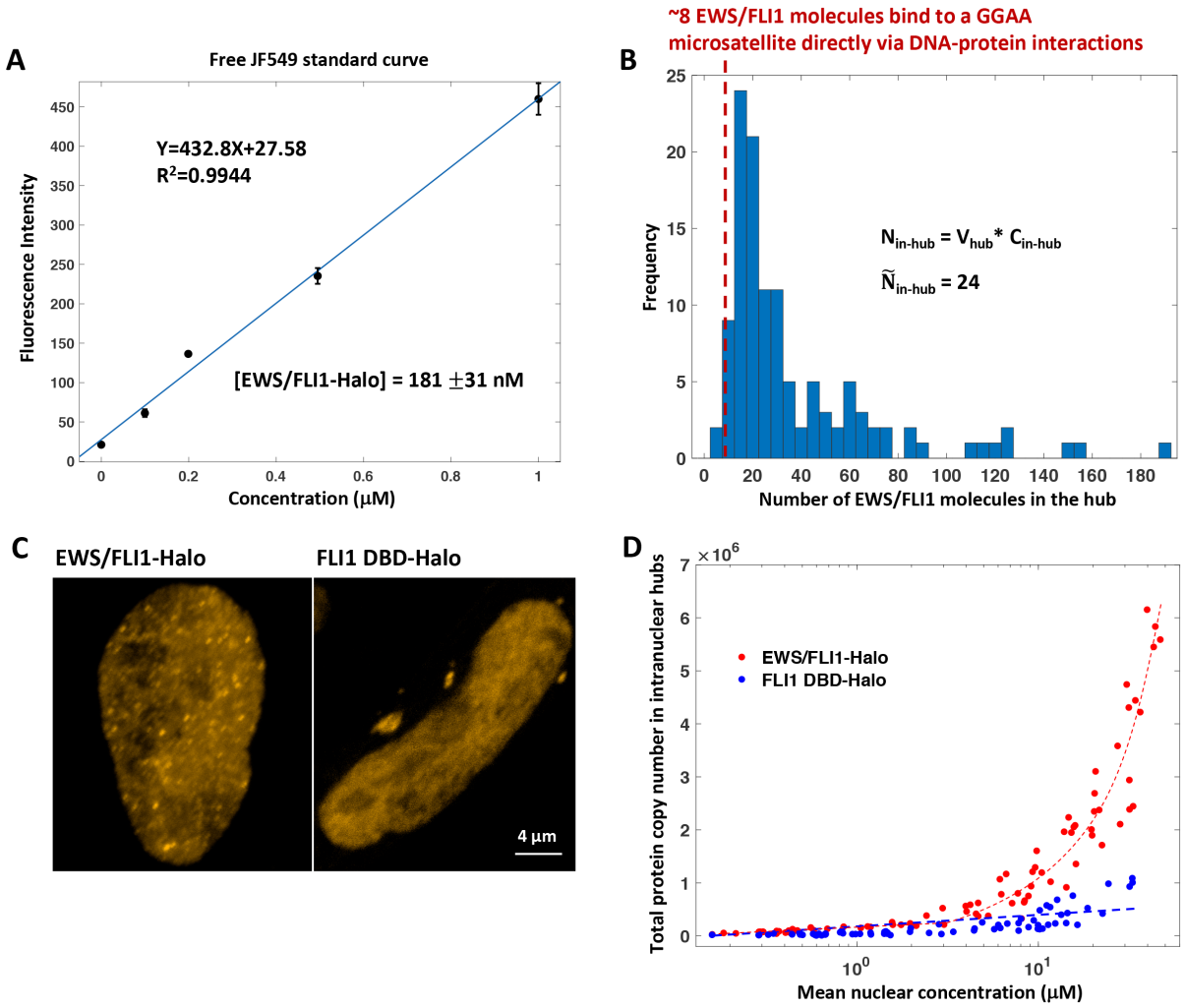

Fig. S7. Intranuclear distribution of EWS/FLI1

(**A**) Fluorescence intensity as a function of free HaloTag ligand JF549 concentration measured by the imaging method shown in Fig. S1A. Error bars represent standard errors. By comparing the nuclear fluorescence intensity of endogenous EWS/FLI1-Halo in A673 cells (labeled with 200 nM JF549) with this standard concentration curve, we estimated the nuclear concentration of the TF to be 181 ± 31 nM. The error bar represents standard deviation. The nuclear concentration is also confirmed by FCS measurement.

(**B**) Distribution of the endogenous EWS/FLI1 copy number per hub at GGAA microsatellites. The median number of EWS/FLI1 molecules directly binding to a GGAA microsatellite via DNA-protein interactions is 8 (red dashed line). The mean concentration of 120 hubs randomly chosen from five A673 cells were measured by fluorescence intensity comparison. (inner equation) The protein copy number in each hub $N_{in\text{-}hub}$ was estimated using the in-hub concentration $C_{in\text{-}hub}$ and the hub volume V_{hub}. We estimated V_{hub} by assuming the hub is a sphere with a radius measured from single cell images. The median copy number of EWS/FLI1 per hub is 24, significantly larger than what is recruited to a GGAA microsatellite via DNA-protein interactions.

(**C**) Confocal fluorescence images of EWS/FLI1-Halo or FLI1 DBD-Halo transiently expressed in U2OS cells. The cells were labeled with HaloTag ligand JF549 (200 nM). At comparable expression levels, EWS/FLI1 forms more distinct hubs in the cell nucleus than FLI1 DBD. (**D**) Total copy number of EWS/FLI1-Halo (red) or FLI1 DBD-Halo (blue) in all the intranuclear hubs as a function of mean nuclear concentration of the TF. Concentrations and copy numbers were measured by fluorescence intensity comparison. Each dot represents one cell. The EWS/FLI1-Halo hubs were defined using the "Find Maxima" function of the ImageJ program *(49)* with a noise tolerance level determined by eye-balling that allows all the intranuclear hubs to be selected as local maxima. The FLI1-Halo hubs in each cell nucleus were defined by the "Find Maxima" function with the noise tolerance used for analyzing cells expressing comparable levels of EWS/FLI1-Halo. EWS/FLI1 hubs enrich more molecules than FLI1 DBD hubs, suggesting that the EWS/FLI1 hubs involve LCD-LCD interactions.

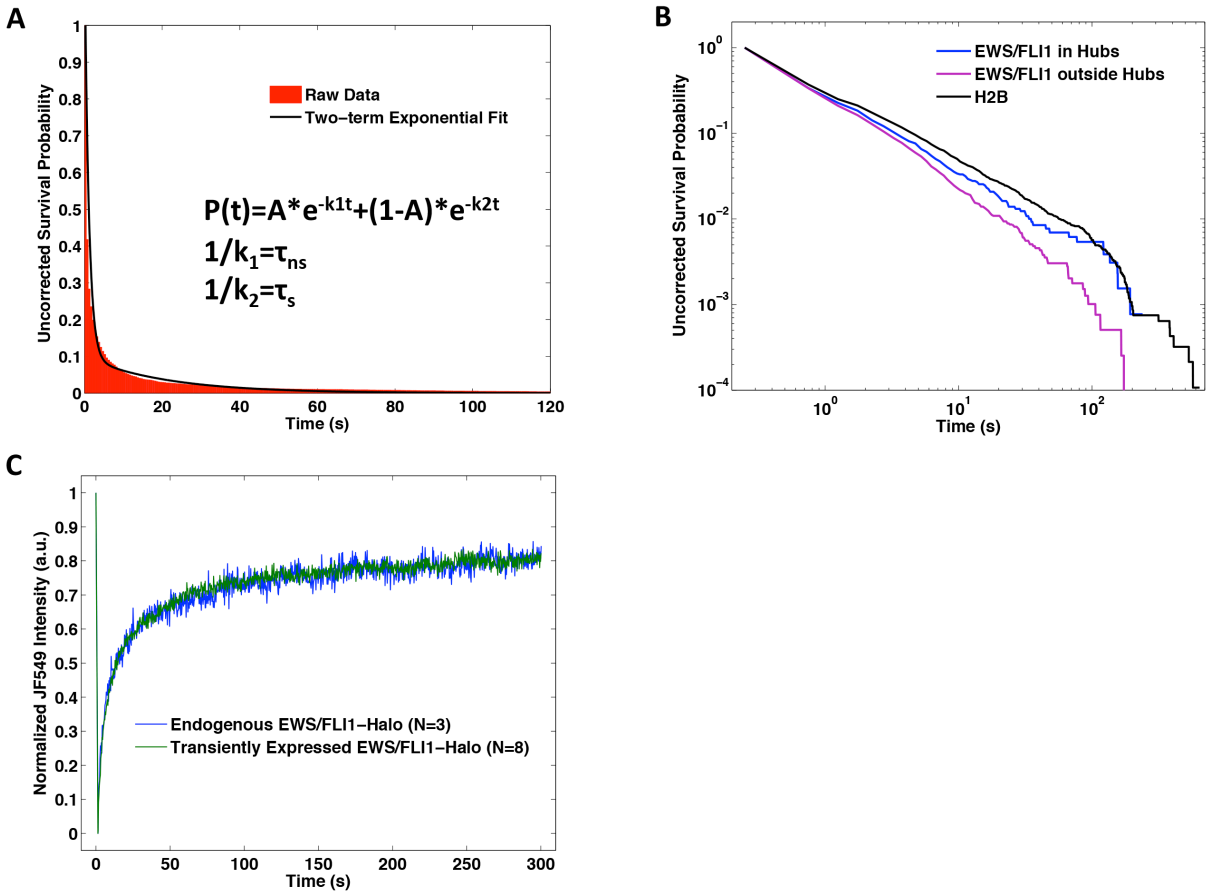

Fig. S8. Live-cell DNA-binding dynamics of EWS/FLI1

(**A**) A plot of the uncorrected survival probability of individual EWS/FLI1-Halo (PA-JF646 labeled) molecules determined by live-cell SPT (red bars), which is fitted to a two-term exponential model (black line, inner equation) that extracts EWS/FLI1 residence times (RTs) for specific (τ_s) and nonspecific (τ_{ns}) DNA binding.

(**B**) Uncorrected survival probability as a function of time for EWS/FLI1 in or outside its hubs. The survival probability of the chromatin bound H2B is plotted as a comparison. The measurement of H2B RT is used to correct EWS/FLI1 RTs for drift and dye photobleaching.

(**C**) The FRAP dynamics of endogenous EWS/FLI1-Halo in knock-in A673 are comparable to transiently expressed EWS/FLI1-Halo in knockout A673. The cells were labeled with HaloTag ligand JF549 (200 nM).

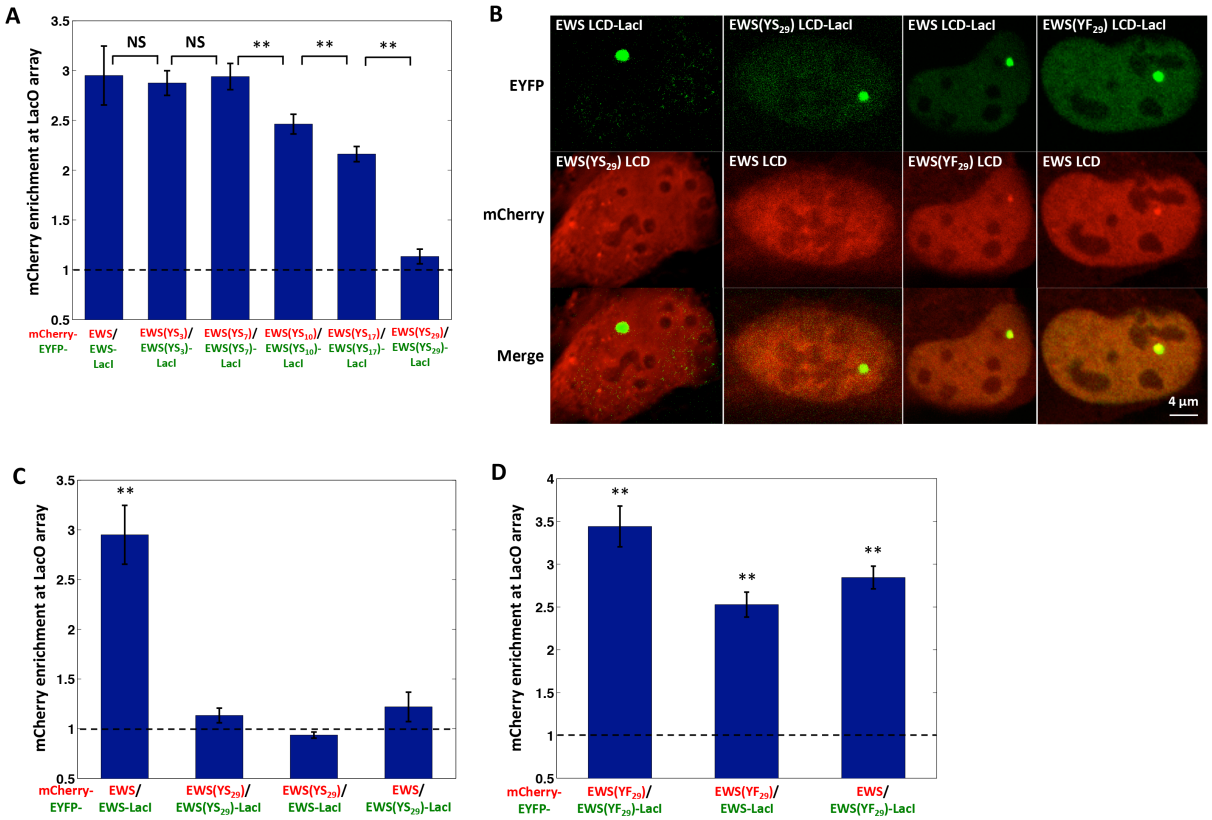

Fig. S9. Y-to-S but not Y-to-F mutations in the EWS LCD abolish LCD-LCD interactions
(**A**) Quantification of the enrichment of mCherry-labeled LCD (font color: red) at the LacO array bound by EYFP labeled LCD-LacI fusion proteins (font color: green), where the LCD is either wild-type EWS or EWS with m = 3, 7, 10, 17 or 29 Y-to-S mutations (YS_m). mCherry enrichment above 1 suggests LCD-LCD interactions at the LacO array. LCD-LCD interactions progressively decrease with increasing number of Y-to-S mutations starting from m = 10. **: $p < 0.01$, two-sample t-test. NS: non-statistically significant difference. Error bars represent standard errors.
(**B**) EWS(YS_{29}) LCD is not enriched at the LacO array bound by EWS LCD-LacI, and conversely, EWS LCD is not enriched at the array bound by EWS(YS_{29}) LCD-LacI, suggesting that EWS and EWS(YS_{29}) LCDs do not interact with each other. On the contrary, EWS and EWS(YF_{29}) LCDs interact with each other.
(**C-D**) Quantification of the enrichment of mCherry-labeled LCD (font color: red) at the LacO array bound by EYFP labeled LCD-LacI fusion proteins (font color: green), where the LCD is either EWS, EWS(YS_{29}) (**C**) or EWS(YF_{29}) (**D**). mCherry enrichment above 1 suggests LCD-LCD interactions at the LacO array. **: statistically significant difference above 1 ($p < 0.01$, one-sample t-test). Error bars represent standard errors.

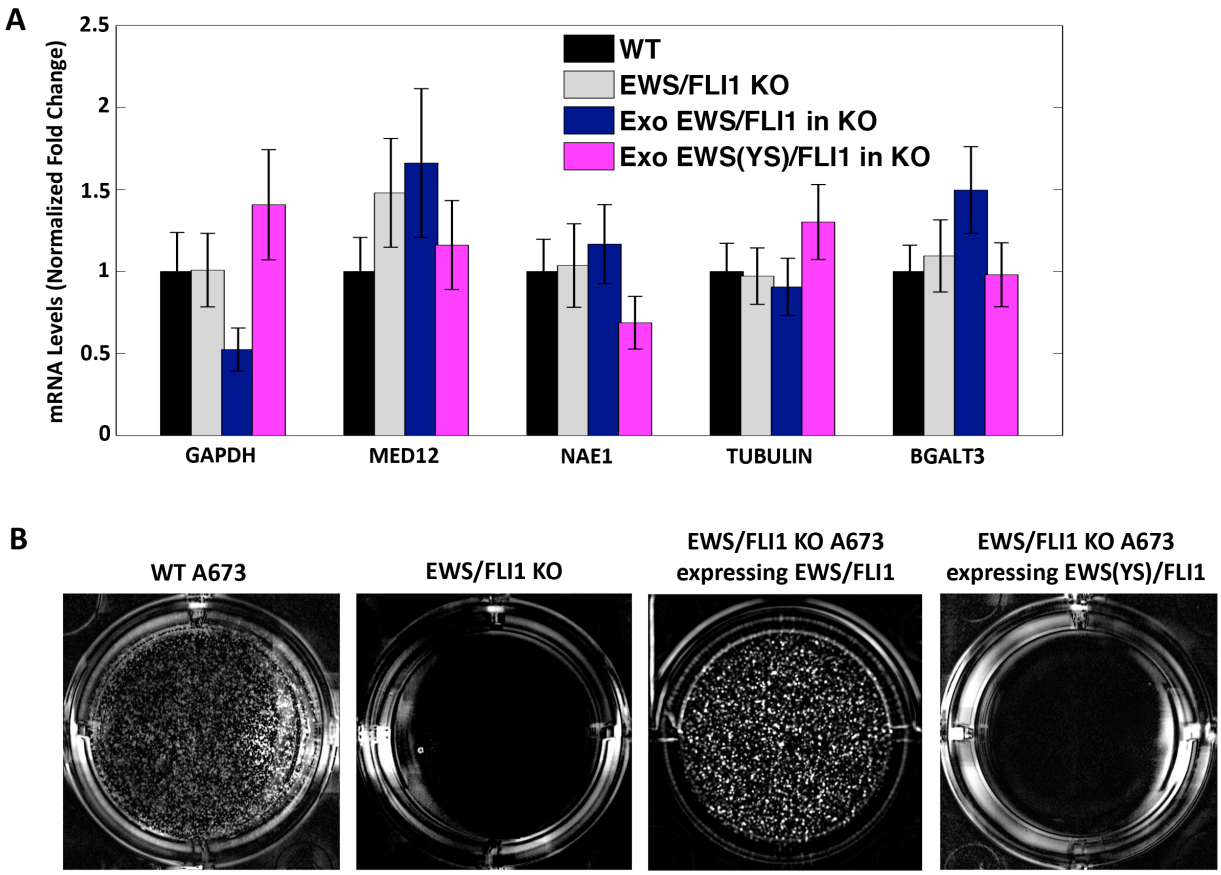

Fig. S10. Assays for studying effects of Y-to-S mutations in the EWS LCD on EWS/FLI1 functions

(**A**) RT-qPCR measures the mRNA levels of 5 different invariant genes in WT A673, EWS/FLI1 KO A673 and the EWS/FLI1 KO lines that stably express exogeneous (Exo) EWS/FLI1 or EWS(YS)/FLI1. For each invariant gene, the mRNA level is graphed as a fold change relative to the amount of RNA present in the WT A673 line (set to 1). Error bars represent standard deviations (n = 5). For each EWS/FLI1-target gene (Fig. 5H), its normalized level of expression is calculated by normalizing its mRNA level with the mRNA level averaged from the 5 invariant genes shown here.

(**B**) Soft agar colony formation assay to examine the cancerous transformation capacity of EWS(YS)/FLI1. EWS/FLI1 KO A673 cells stably expressing exogenous EWS/FLI1, but not EWS(YS)/FLI1, are able to form colonies in agar. As controls, WT but not EWS/FLI1 KO A673 cells grow in agar. This result shows that Y-to-S mutations abolish the cancerous transformation capacity of EWS/FLI1.

Table S1. Amino acid composition of FET and Sp1 LCDs studied with the LacO array assay

Protein		EWS	FUS	TAF15	Sp1
LCD residues		47-266	2-214	2-205	2-507
Percentage of individual amino acid (%)	Ala (A)	8.6	1.9	1.0	7.3
	Arg (R)	0.5	0.5	4.3	1.2
	Asn (N)	1.8	3.3	4.8	7.5
	Asp (D)	1.8	2.3	8.2	1.3
	Cys (C)	0.0	0.0	0.0	0.2
	Gln (Q)	16.7	20.0	17.3	14.6
	Glu (E)	0.9	0.5	3.8	3.7
	Gly (G)	9.0	24.7	18.3	11.5
	His (H)	0.0	0.0	2.4	0.2
	Ile (I)	0.0	0.0	0.0	5.0
	Leu (L)	0.5	0.0	0.0	7.1
	Lys (K)	0.5	0.0	1.0	1.0
	Met (M)	0.5	0.5	1.0	1.3
	Phe (F)	0.0	0.0	0.0	1.3
	Pro (P)	13.1	5.1	2.4	5.0
	Ser (S)	16.2	23.7	18.8	14.4
	Thr (T)	14.9	5.1	3.4	10.8
	Trp (W)	0.0	0.0	0.0	0.4
	Tyr (Y)	13.1	12.6	13.0	0.8
	Val (V)	2.3	0.0	0.5	5.4
	Pyl (O)	0.0	0.0	0.0	0.0
	Sec (U)	0.0	0.0	0.0	0.0

Table S2. P-values determined by one-tailed Student's t-test

Related figure	Alternative hypothesis	P-value
Fig. 1G	Average Halo-RPB1 enrichment by EWS LCD-LacI at the LacO array is greater than by LacI	0 (too small to be reported by Matlab)
	Average Halo-RPB1 enrichment by FUS LCD-LacI at the LacO array is greater than by LacI	0 (too small to be reported by Matlab)
	Average Halo-RPB1 enrichment by TAF15 LCD-LacI at the LacO array is greater than by LacI	0 (too small to be reported by Matlab)
Fig. 2B	mCherry-TAF15 enrichment at the LacO array bound by EYFP-TAF15-LacI is greater than 1	9.3024e-14
	mCherry-FUS enrichment at the LacO array bound by EYFP-FUS-LacI is greater than 1	7.6749e-07
	mCherry-EWS enrichment at the LacO array bound by EYFP-EWS-LacI is greater than 1	2.2562e-07
	mCherry-Sp1 enrichment at the LacO array bound by EYFP-Sp1-LacI is greater than 1	3.7129e-04
	mCherry-EWS enrichment at the LacO array bound by EYFP-TAF15-LacI is greater than 1	5.8369e-04
	mCherry-FUS enrichment at the LacO array bound by EYFP-TAF15-LacI is greater than 1	0.0449
	mCherry-TAF15 enrichment at the LacO array bound by EYFP-FUS-LacI is greater than 1	0.0026
	mCherry-FUS enrichment at the LacO array bound by EYFP-EWS-LacI is greater than 1	0.0452
	mCherry-TAF15 enrichment at the LacO array bound by EYFP-EWS-LacI is greater than 1	0.0165
Fig. 3B	Residence time of EWS LCD in LacO-associated EWS-LacI hubs is greater than in self-aggregated EWS LCD hubs	0.0081
	Residence time of FUS LCD in LacO-associated FUS-LacI hubs is greater than in self-aggregated FUS LCD hubs	0.0129
Fig. 5B	Residence time in hubs is longer than outside hubs	1.8059e-08
Fig. 5D	Residence time of EWS/FLI1 in hubs is longer than EWS(YS)/FLI1	0.0159
	Residence time of EWS/FLI1 in hubs is longer than FLI1-DBD	6.9710e-04
Fig. 5F	Residence time of EWS LCD in EWS/FLI1 hubs is longer than EWS(YS) LCD	0.0320
Fig. 5G	GGAA-containing reporter is activated by EWS/FLI1 more efficiently than EWS(YS)/FLI1	4.3159e-06
	GGAA-containing reporter is activated by EWS/FLI1 more efficiently than FLI1-DBD	2.5010e-05
Fig. 5H	*FCGRT* expression in the WT A673 is higher than EWS/FLI1 KO A673	9.8124e-05

	FCGRT expression in the Exo EWS/FLI1 condition is higher than Exo EWS(YS)/FLI1 condition	0.0032
	CYP4F22 expression in the WT A673 is higher than EWS/FLI1 KO A673	1.7125e-07
	CYP4F22 expression in the Exo EWS/FLI1 condition is higher than Exo EWS(YS)/FLI1 condition	1.8769e-07
	CCK expression in the WT A673 is higher than EWS/FLI1 KO A673	5.6432e-09
	CCK expression in the Exo EWS/FLI1 condition is higher than Exo EWS(YS)/FLI1 condition	1.7689e-06
	FEZF1 expression in the WT A673 is higher than EWS/FLI1 KO A673	2.5088e-07
	FEZF1 expression in the Exo EWS/FLI1 condition is higher than Exo EWS(YS)/FLI1 condition	5.5223e-05
	NKK2-2 expression in the WT A673 is higher than EWS/FLI1 KO A673	0.0288
	NKK2-2 expression in the Exo EWS/FLI1 condition is higher than Exo EWS(YS)/FLI1 condition	0.0304
	CACNB2 expression in the WT A673 is higher than EWS/FLI1 KO A673	4.7444e-07
	CACNB2 expression in the Exo EWS/FLI1 condition is higher than Exo EWS(YS)/FLI1 condition	1.0687e-04
	GSTM4 expression in the WT A673 is higher than EWS/FLI1 KO A673	8.9997e-09
	GSTM4 expression in the Exo EWS/FLI1 condition is higher than Exo EWS(YS)/FLI1 condition	8.5400e-05
	PPP1R1A expression in the WT A673 is higher than EWS/FLI1 KO A673	8.2648e-10
	PPP1R1A expression in the Exo EWS/FLI1 condition is higher than Exo EWS(YS)/FLI1 condition	7.3388e-05
	NR0B1 expression in the WT A673 is higher than EWS/FLI1 KO A673	4.3640e-04
	NR0B1 expression in the Exo EWS/FLI1 condition is higher than Exo EWS(YS)/FLI1 condition	6.0396e-06
	KDSR expression in the WT A673 is higher than EWS/FLI1 KO A673	5.3393e-04
	KDSR expression in the Exo EWS/FLI1 condition is higher than Exo EWS(YS)/FLI1 condition	7.3582e-04
	ABHD6 expression in the WT A673 is higher than EWS/FLI1 KO A673	3.3504e-09
	ABHD6 expression in the Exo EWS/FLI1 condition is higher than Exo EWS(YS)/FLI1 condition	0.0025
	BAF155 expression in the Exo EWS/FLI1 condition is higher than Exo EWS(YS)/FLI1 condition	2.9416e-04
	EZH2 expression in the WT A673 is higher than EWS/FLI1 KO A673	0.0367

	EZH2 expression in the Exo EWS/FLI1 condition is higher than Exo EWS(YS)/FLI1 condition	0.0047
	PRKCB expression in the WT A673 is higher than EWS/FLI1 KO A673	1.1705e-04
	PRKCB expression in the Exo EWS/FLI1 condition is higher than Exo EWS(YS)/FLI1 condition	2.7318e-06
	UGT3A2 expression in the WT A673 is higher than EWS/FLI1 KO A673	1.3304e-07
	UGT3A2 expression in the Exo EWS/FLI1 condition is higher than Exo EWS(YS)/FLI1 condition	5.6997e-06
Fig. S6C	GGAA-containing reporter is activated by EWS/FLI1 more efficiently than empty vector	8.1950e-04
	GGAA-containing reporter is activated by EWS/FLI1-Halo more efficiently than empty vector	0.0020
Fig. S6E	WT A673 cells form greater number of colonies than EWS/FLI1 KO A673	1.7164e-07
	EWS/FLI1-Halo KI A673 cells form greater number of colonies than EWS/FLI1 KO A673	6.2759e-09
Fig. S9A	mCherry-EWS(YS_7) enrichment at the LacO array bound by EYFP-EWS(YS_7)-LacI is greater than mCherry-EWS(YS_{10}) enrichment at the LacO array bound by EYFP-EWS(YS_{10})-LacI	0.0032
	mCherry-EWS(YS_{10}) enrichment at the LacO array bound by EYFP-EWS(YS_{10})-LacI is greater than mCherry-EWS(YS_{17}) enrichment at the LacO array bound by EYFP-EWS(YS_{17})-LacI	0.0078
	mCherry-EWS(YS_{17}) enrichment at the LacO array bound by EYFP-EWS(YS_{17})-LacI is greater than mCherry-EWS(YS_{29}) enrichment at the LacO array bound by EYFP-EWS(YS_{29})-LacI	1.9347e-07
Fig. S9C	mCherry-EWS enrichment at the LacO array bound by EYFP-EWS-LacI is greater than 1	2.2562e-07
Fig. S9D	mCherry-EWS(YF_{29}) enrichment at the LacO array bound by EYFP-EWS(YF_{29})-LacI is greater than 1	9.0988e-14
	mCherry-EWS(YF_{29}) enrichment at the LacO array bound by EYFP-EWS-LacI is greater than 1	1.5186e-14
	mCherry-EWS enrichment at the LacO array bound by EYFP-EWS(YF_{29})-LacI is greater than 1	4.2377e-20

Table S3. Sequences for primers and sgRNAs used in genome editing of A673 cells

Name/description	Sequence (5'-3')	Experiment
FLI1 C-terminal sgRNA1	ACGTGCCTTCACACTTAGGC	EWS/FLI1-Halo Knock-in
FLI1 C-terminal sgRNA2	CGTGCCTTCACACTTAGGCA	
FLI1 C-terminal sgRNA3	ACCCACGTGCCTTCACACTT	
FLI1 genome F1	TTCAGGCCTTTCTAGATGAA GAGATTCAAA	Genotyping
Internal Halo primer R1	TCGCCCAGGACTTCCACATA ATGG	
EWS N-terminal sgRNA1	CGGGTGAGTATGGTGGAACT	EWS/FLI1 Knockout
EWS N-terminal sgRNA2	GGAGAGAAAATGGCGTCCAC	

Table S4. Sequences for primers used in RT-qPCR

Name/description	Sequence (5'-3')	Experiment
Primers targeting *FCGRT*	TGGCGATGAGCACCACTACT	Quantification of mRNA levels of GGAA-microsatellite-associated EWS/FLI1 target genes in wild-type and modified A673 lines
	GGAGGACTTGGCTGGAGATT	
Primers targeting *CYP4F22*	ATATCCGAGCCGAAGCAGACAC	
	CGGCATTTCTCCTGGTATTCCG	
Primers targeting *UGT3A2*	TGTTGGAGGCTTGATGGAAAAACC	
	CGGATTCTGACAGGTGTTCACC	
Primers targeting *CCK*	TGAGGGTATCGCAGAGAACGGA	
	CGGTCACTTATCCTGTGGCTGG	
Primers targeting *PPP1R1A*	CACAGAAGTGGAGTCAAGGCTG	
	TTGGCTCCCTTGGAATCCAGTG	
Primers targeting *NR0B1*	AGGGGACCGTGCTCTTTAAC	
	CTGAGTTCCCCACTGGAGTC	
Primers targeting *FEZF1*	TTCAGCCGAGGCTCTCCTAATG	
	GCCTGAAACCTTTTCCGCACAC	
Primers targeting *NKX2-2*	CAGCGACAACCCGTACAC	
	GACTTGGAGCTTGAGTCCTGA	
Primers targeting *PRKCB*	GAGGGACACATCAAGATTGCCG	
	CACCAATCCACGGACTTCCCAT	
Primers targeting *EZH2*	TGGGAAAGTACACGGGGATA	
	TATTGACCAAGGGCATTCAC	
Primers targeting *GAPDH*	GGTCTCCTCTGACTTCAACA	
	GTGAGGGTCTCTCTCTTCCT	
Primers targeting *BAF155*	GAGAATGGACTGAACAGGAGACC	
	GGGTCCTCAATGGGAAGTCTCA	
Primers targeting *ABHD6*	CTTGGTCTGCGTGGACAT	
	GCTTCAGGCATTCTACAAA	
Primers targeting *KDSR*	GGATGGCTCCAGTAACTTC	
	ACGAACTATGCTGTCAAAAC	
Primers targeting *CACNB2*	CACCCTAGCCTCTAATTCAC	
	TCTTGACTGGTTCCACACTA	
Primers targeting *GSTM4*	CCAGAATACTTGGAGGAACT	
	TCATAGGCGAGGAAATCTAC	
Primers targeting *TUBULIN*	TTTTGGCCAGATCTTTAGAC	
	ACATCCAGGACAGAATCAAC	
Primers targeting *MED12*	CTTTGGTCCGGCAACTTC	
	TATGTTGGTACTGGGCTGTG	
Primers targeting *NAE1*	GATCGCTGCATAAATATCAC	

	AAATTTCCTTGACCCTCTTT	
Primers targeting *BGALT3*	CCGTTGCTATGAACAAGTTT	
	GCCATTCATCTTCAGGTACT	
Primers targeting beginning of LacO repeats-containing plasmid	ACGGCCAGTGAATTGTAA	Estimating the number of LacO repeats in each LacO array
	GGGGGATCCACTAGTTCT	
Primers targeting end of LacO repeats-containing plasmid	CAGCTTTTGTTCCCTTTAGT	
	ATGTTGTGTGGAATTGTGAG	

Table S5. RT-qPCR results for LacO repeat number quantification

LacO array in the tested cell line	Target of primer pair	Target copy number in 10 ng of gDNA by qPCR	Copy number of target per genome (6 pg gDNA)	Number of LacO repeats per plasmid	Number of LacO repeats per genome normalized by globin gene number
2	Before LacO repeats on the array-containing plasmid	101235	60.74	256	13331
2	After LacO repeats on the array-containing plasmid	129306	77.58	256	17027
2	Globin gene	3888	2.33	/	/
3	Before LacO repeats on the array-containing plasmid	1979170	1187.50	40	35474
3	After LacO repeats on the array-containing plasmid	2572921	1543.75	40	46116
3	Globin gene	4463	2.68	/	/

On average, LacO arrays 2 and 3 contain 15179 and 40795 LacO repeats, respectively.

Movie S1. LacO-array-associated and self-aggregated non-array-affiliated FUS LCD hubs in live cells are quickly disrupted by 10% 1,6-hexanediol (related to Fig. 2C).

Movie S2. 360° view of a 3D image of endogenous EWS/FLI1-Halo in an A673 cell nucleus (stained with 200 nM Halo ligand JF549) taken on the lattice light sheet microscope (related to Fig. 4C).

Movie S3. Two-color movie imaging endogenous EWS/FLI1-Halo in knock-in A673 cell nucleus stained with two HaloTag ligands, JF549 (200 nM) and PA-JF646 (20 nM). The image acquisition time was 500 ms. We took time-lapse images with a 10 sec interval in the JF549 channel to visualize EWS/FLI1 hubs, and imaged continuously in the PA-JF646 channel for SPT of individual EWS/FLI1-Halo molecules (related to Fig. 5A).

Supplemental References:

46. F. Mueller *et al.*, FISH-quant: automatic counting of transcripts in 3D FISH images. *Nat. Methods.* **10**, 277-278 (2013).

47. I. I. Cisse *et al.*, Real-time dynamics of RNA polymerase II clustering in live human cells. *Science.* **341**, 664-667 (2013).

48. S. Sankar *et al.*, EWS and RE1-Silencing Transcription Factor Inhibit Neuronal Phenotype Development and Oncogenic Transformation in Ewing Sarcoma. *Genes Cancer.* **4**, 213-223 (2013).

49. C. A. Schneider, W. S. Rasband, K. W. Eliceiri, NIH Image to ImageJ: 25 years of image analysis. *Nat. Methods.* **9**, 671-675 (2012).

50. E. Garimberti, S. Tosi, Fluorescence in situ hybridization (FISH), basic principles and methodology. *Methods Mol. Biol.* **659**, 3-20 (2010).

51. M. Tokunaga, N. Imamoto, K. Sakata-Sogawa, Highly inclined thin illumination enables clear single-molecule imaging in cells. *Nat. Methods.* **5**, 159-161 (2008).

52. A. Serge, N. Bertaux, H. Rigneault, D. Marguet, Dynamic multiple-target tracing to probe spatiotemporal cartography of cell membranes. *Nat. Methods.* **5**, 687-694 (2008).

53. D. Normanno *et al.*, Probing the target search of DNA-binding proteins in mammalian cells using TetR as model searcher. *Nat. Commun.* **6**, 7357 (2015).

54. S. S. Teves *et al.*, A dynamic mode of mitotic bookmarking by transcription factors. *Elife.* **5**, 10.7554/eLife.22280 (2016).

55. D. Mazza, A. Abernathy, N. Golob, T. Morisaki, J. G. McNally, A benchmark for chromatin binding measurements in live cells. *Nucleic Acids Res.* **40**, e119 (2012).